Talanta 129 (2014) 241–248

Contents lists available at ScienceDirect

Talanta

journal homepage: www.elsevier.com/locate/talanta

A two-photon ratiometric fluorescent probe enables spatial coordinates determination of intracellular pH

Junjie Wang [a], Yuming Sun [b], Weijia Zhang [a], Yong Liu [a], Xiaoqiang Yu [a,*], Ning Zhao [c,**]

[a] Center of Bio & Micro/Nano Functional Materials, State Key Laboratory of Crystal Materials, Shandong University, Jinan 250100, PR China
[b] School of Information Science and Engineering, Shandong University, PR China
[c] Key Laboratory for Adhesion & Sealing Materials of Shandong Province, New Material Institute of Shandong Academy of Sciences, Jinan 250014, Shandong, China

ARTICLE INFO

Article history:
Received 24 January 2014
Received in revised form
14 May 2014
Accepted 20 May 2014
Available online 29 May 2014

Keywords:
Two-photon
Fluorescent probe
Ratiomatric
Intracellular pH
Bioimaging

ABSTRACT

We reported a two-photon ratiometric fluorescent probe for detecting intracellular pH. When excited with 800 nm laser, an optimal output of laser as the routine equipment of two-photon fluorescence microscopy, the two-photon excited fluorescence of this probe showed distinct emission peak shift as large as 109 nm upon the change of pH values in vitro. Very importantly, the experiment results show that this probe has large two-photon absorption cross-section at pH 4.5 at 800 nm of 354 g, which ranks it as one of the best two-photon ratiometric fluorescent pH probes, and its working pH value is between 4.0 and 8.0 which could fit the intracellular pH range. Moreover, utilizing this probe, the two-photon ratiometric fluorescent images in living cells have been obtained, and the spatial coordinates of intracellular pH can be mapped. At the same time, the probe also exhibited selectivity, photostability and membrane permeability. And the photophysical properties of this probe in various solvents indicated that these photophysical properties variations are due to an intramolecular charge transfer process. At last, the imaging depth of the probe in liver biopsy slices was investigated. The experimental results demonstrated the maximum imaging depth can arrive 66 μm in living rat liver tissues.

1. Introduction

Intracellular pH plays an essential role in regulating many cellular processes [1]. Moreover, abnormality of the intracellular pH may lead to dysfunction of the organelles [2,3]. Thus, in order to detect intracellular pH, various turn-on or ratiometric fluorescent probes have been developed extensively [4,5]. Among, ratiometric probes that can perform a built-in correction of two emission bands consequently eliminate distortions of data caused by photobleaching, nonuniform probes distribution within cells and variations in probe loading and retention as well as by instrumental factors such as illumination stability, have been evolved intensively [6,7]. Relevant research works indicated that ratiometric probes possess unique advantage on imaging intracellular different physiological parameters such as pH and viscosity [8–10].

Recently, a comparison study convincingly demonstrated that two-photon fluorescence microscopy (TPM) is superior to confocal one when imaging living and thick specimen due to its lower background signals, high detection sensitivity, no image distortion, low photodamage and photobleaching [11]. However, if the two-photon excited fluorescence (TPEF) properties of biological probes are smaller or comparable with endogenous fluorophores in a specimen, TPEF from endogenous fluorophores will interfere the TPEF imaging of probes. Thus, in order to obtain usable TPEF photos, the TPEF of biological probes should be stronger than that of endogenous fluorophores under the same excitation conditions, namely, TPEF properties of the probes should be better than that of endogenous fluorophores in a specimen [12]. Thus, the design and synthesis of biological fluorescence probes with good TPEF properties is an active research area.

So far, some two-photon ratiometric fluorescent (TPRF) pH probes have been reported and a few enables living cell/tissue imaging [13–18]. For example, Park et al. [14] reported a TPRF probe with a peak shift upon the change of pH and relevant tissue bioimaging. Jobsis et al. [15] carried out TPEF pH detection in living primary mouse embryo fibroblasts using a commercial membrane permeability ratiometric probe (DCHQ) and tested its TPEF properties. Esipova et al. [16] developed a series of upconversion fluorescent nanoparticles with excellent ratiometric properties upon the change of pH between 6.0 and 8.0. However, because nanoparticles do not possess the permeability to intact cell membrane, they must be introduced into living cells by the

* Corresponding author. Tel.: +86 531 883 66418.
** Corresponding author.
E-mail addresses: yuxq@sdu.edu.cn (X. Yu), zhaon@sdas.org (N. Zhao).

http://dx.doi.org/10.1016/j.talanta.2014.05.039
0039-9140/

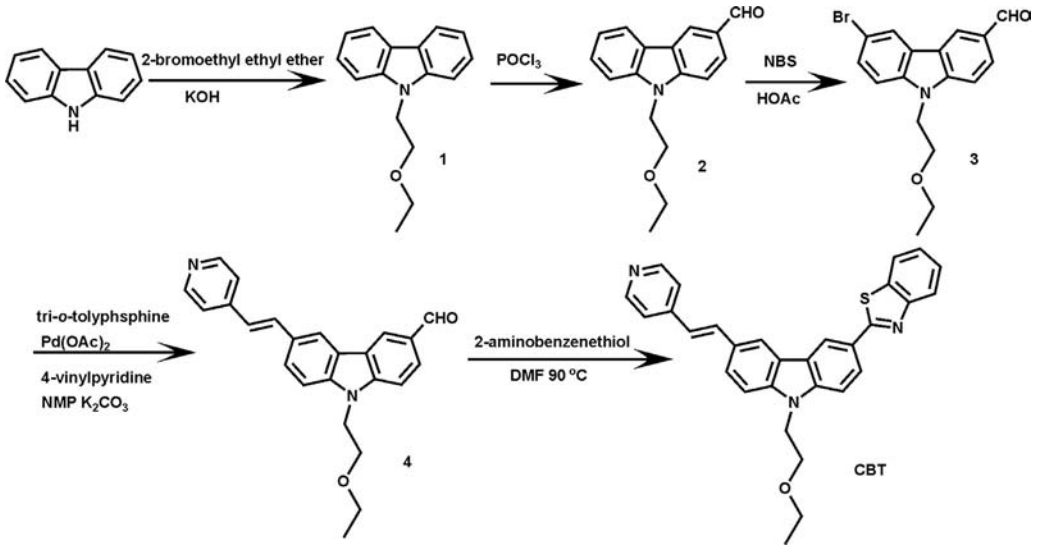

Scheme 1. Synthesis of CBT.

microinjection which is destructive to cell and cannot maintain the physiological and structural integrity of the cell. Yao et al. [17] gave a near neutral pH indicator and realized the cell imaging, and the TPEF spectra in different pH were not plotted. More recently, Kim et al. [18] reported a family of TPRF probes for acid pH in live cell and tissue, and one optimized can target lysosome and may estimate pH value inside lysosomal compartments. But, so far, a TPRF probe by which the intracellular pH spatial coordinates can be obtained is still little.

In previous research works, we reported various TPEF probes targeting different entities, such as DNA, RNA, cysteine [19–21]. Especially, we have synthesized a one-photon ratiometric fluorescent pH probe 3-acetyl-6-(4-vinylpyridine)-9-ethyl-carbazole (CAE) based on the pyridine and carbazole and utilized it to image the acidic compartments in living cells; moreover it is also a good two-photon turn-on probe [22]. Herein, we assembled the pyridine, carbazole and benzothiazole rationally and then synthesized a new TPRF probe 2-(9-(2-ethoxyethyl)-6-(2-(pyridin-4-yl)vinyl)-carbazol-3-yl)benzo[*d*]thiazole (CBT, Scheme 1) with larger conjugated extent in comparison with CAE. The experiment results showed that this probe possesses two unique advantages. First, compared with some TPRF probes reported, the GM value of 354 at pH 4.5, which quantifies the efficiency of TPEF for different fluorescent probes, can rank it as one of the best TPRF pH probes. Second, as a TPRF probe, the TPEF of CBT can show distinct emission peak shift as large as 109 nm upon the change of pH values, so that two well-separated fluorescent detection channels (I: 430–480 nm and II: 525–575 nm) can be carried out by the radiometric fluorescent imaging, which can avoid the image distortion resulted from fluorescence cross color. At the same time, the results from in situ calibration in living cells [4,5] show that the spatial coordinates of intracellular pH can also be mapped. Moreover, the imaging depth of the probe in liver biopsy slices was investigated. And the maximum imaging depth can arrive 66 μm in living rat liver tissues.

2. Experimental

2.1. Chemicals and instrumentation

Carbazole and N-bromosuccinimide (NBS) were purchased from Sinopharm Chemical Reagent Co., Ltd (Shanghai, China). Palladium (II) acetate, 4-vinylpyridine, tri-*o*-tolylphosphine and 3-(4,5-dimethyl-2-thiazolyl)-2,5-diphenyltetrazolium bromide (MTT) were purchased from J&K Chemical (Beijing, China). 2-aminobenzenethiol was purchased from Aladdin Co. All solvents used for synthesis and measurements were redistilled before they were used. All other chemicals were of analytical-reagent grade (purity ≥ 99.5%) and were used without further purification. Ultrapure water was used throughout. The thin layer chromatography (TLC) analyses were performed on silica gel plates and column chromatography was conducted over silica gel (mesh 200–300), both of which were obtained from Qingdao Ocean Chemicals. Nuclear magnetic resonance spectra (^{1}HNMR and ^{13}CNMR) were obtained using a Bruker Avanace 300/400 spectrometer. The high resolution mass spectrometer (HRMS) spectra were recorded on Agilent Technologies 6510 Q-TOF LC/MS. The UV–visible-near-IR absorption spectra of dilute solutions were recorded using a HITACHI U-2910 spectrophotometer. One-photon fluorescence spectra were obtained using a HITACHI F-2700 spectrofluorimeter equipped with a 450 W Xe lamp. Two-photon excited fluorescence spectra were recorded using a SpectroPro300i and the pump laser beam comes from a mode-locked Ti: sapphire laser system at the pulse duration of 200 fs, with a repetition rate of 76 MHz (Coherent Mira900-D). All pH measurements were performed with a METTLER TOLEDO FE20-FiveEasy™ pH-meter. Two-photon fluorescence imaging was obtained with a LSM 710 NLO (Zeiss) multiphoton laser scanning microscope. Confocal fluorescence imaging was obtained with a LSM 780 (Zeiss) confocal laser scanning microscope.

2.2. Synthesis of 2-(9-(2-ethoxyethyl)-6-(2-(pyridin-4-yl)vinyl)-carbazol-3-yl)benzo[d]thiazole (CBT)

The synthesis of CBT was with facile and economic methods. The intact synthesis process needs five steps shown in Scheme 1. All approaches do not require some expensive and dangerous techniques such as high temperature, high pressure and high vacuum. Step 1–4 have been described in Supporting information, Final step was as follows. A mixture of compounds 4 (0.37 g, 1×10^{-3} mol) and 2-aminobenzenethiol (0.13 g, 1×10^{-2} mol) in 20 mL of DMF were stirred at 90 °C overnight. The mixture was cooled and extracted with 100 mL dichloromethane three times, washed with 200 mL brine three times, dried with anhydrous magnesium sulfate, filtered and concentrated. The crude product was purified on a silica gel column using ethyl acetate as the eluent and the recrystallization from methanol produced light brown crystals CBT. Yield, 44%, 0.21 g; ^{1}HNMR ($CDCl_3$, 300 MHz): δ 8.86 (s, 1H), 8.59 (d, J=6.0 Hz, 2H),

8.36 (s, 1H), 8.21 (dd, J=8.7 Hz, 1.5 Hz, 1H), 8.09 (d, J=7.8 Hz, 1H), 7.92 (d, J=7.8 Hz, 1H), 7.71 (d, J=8.4 Hz, 1H), 7.48 (m, 7H) 7.09 (d, J=16.2 Hz, 1H), 4.51 (t, J=5.5 Hz, 2H), 3.84 (t, J=5.7 Hz, 2H), 3.42 (t, J=7.1 Hz, 2H), 1.10 (t, J=6.9 Hz, 3H) ^{13}CNMR ($CDCl_3$, 75 MHz): δ 169.03, 154.37, 150.04, 145.25, 142.84, 141.67, 134.92, 133.91, 128.37, 126.26, 125.90, 125.67, 125.42, 124.73, 123.76, 123.47, 123.33, 122.75, 121.53, 120.69, 119.97, 119.59, 109.76, 109.70, 77.43, 76.58, 68.57, 66.96, 43.81, 15.10. HRMS: calculated for [M^+] 476.1718, found 476.1808.

2.3. Spectroscopic measurements

All spectra were obtained with 1.0 cm Quartz cells. The concentration of CBT dissolved in Britton-Robinson buffer solution (4×10^{-2} mol L^{-1} H_3BO_3, 4×10^{-2} mol L^{-1} H_3PO_4 and 4×10^{-2} mol L^{-1} CH_3COOH) was 5×10^{-5} mol L^{-1} and its pH values were modified with 0.2 mol L^{-1} NaOH. In order to maintain a constant ionic strength all solutions contain 0.1 mol L^{-1} NaCl and 0.02 mol L^{-1} KCl. The solution was equilibrated for 3 min before measurement.

The fluorescence quantum yields can be calculated by means of Eq. (1):

$$\Phi_s = \Phi_r \left(\frac{A_r(\lambda_r)}{A_s(\lambda_s)}\right)\frac{c_r}{c_s}\frac{n_s^2}{n_r^2}\frac{F_s}{F_r} \quad (1)$$

where the subscripts s and r refer to the sample and the reference materials, respectively. Φ is the quantum yield, F is the integrated emission intensity, A stands for the absorbance, and n is the refractive index. In this paper, the quantum yields were calculated by using quinine sulfate in 0.5 mol L^{-1} H_2SO_4 (Φ=55%) as a standard [23].

Two-photon absorption (TPA) cross sections have been measured using the two-photon induced fluorescence method [24]. Fluorescein in aqueous NaOH (pH 13) was used as the standard, whose two-photon properties have been characterized in the literature, and thus cross sections can be calculated by means of Eq. (2)

$$\delta_s = \delta_r \frac{\Phi_r}{\Phi_s}\frac{c_r}{c_s}\frac{n_r}{n_s}\frac{F_s}{F_r} \quad (2)$$

where the subscripts s and r refer to the sample and the reference materials, respectively. δ is the TPA cross sectional value, c is the concentration of the solution, n is the refractive index of the solution, F is the two-photon excited fluorescence integral intensity and Φ is the fluorescence quantum yield.

2.4. Cell culture and staining

HeLa cells and SiHa cells were grown in H-DMEM supplemented with 10% FBS in a 5% CO_2 incubator at 37 °C. Cells were placed on glass bottom culture (NEST) and allowed to adhere for 24 h. For living cells imaging experiment of CBT, cells were incubated with 2×10^{-6} mol L^{-1} CBT in PBS (2% DMSO, pH 7.4) for 30 min at 37 °C.

2.5. Calibration experiment in SiHa cells

After SiHa cells stained with CBT for 30 min, the cells were washed with PBS. In order to equilibrate intracellular pH values, 1×10^{-6} g mL^{-1} of nigericin (Aldrich, 1×10^{-4} L) then Britton-Robinson buffer solution (9×10^{-4} L) with 4.5 or 6.0 pH were added for 30 min to allow a rapid exchange of K^+ and H^+ which resulted in a rapid equilibration of external and internal pH values. The cells were then analyzed by confocal microscopy as described above.

2.6. Cell viability evaluated by MTT assay

Viability of the cells was assayed using cell proliferation Kit I with the absorbance of 492 nm being detected using a Perkin-Elmer Victor plate reader. Five thousand cells were seeded per well in a 96-well plate. After overnight culture, various concentrations of CBT were added into the 96-well plate. After 2 h treatment, 20 mL of MTT solution (5×10^{-3} g mL^{-1} in phosphate buffer solution) was added into each well. After 4 h incubation at 37 °C, 200 mL DMSO was added to dissolve the purple crystals. After 20 min dissolution, the optical density readings at 492 nm were taken using a plate reader.

2.7. Rat liver biopsy Slices preparation and staining

Sprague-Dawley (SD) rats (14-day-old, SPF) were purchased from the Experimental Animals Center of Tongji Medical College of Huazhong University of Science and Technology. All animal experiments were approved by the Animal Care Committee of Shandong University. Each rat was decapitated, and Liver was isolated quickly from body. The liver biopsy slices were cut into 500 μm-thick using a vibrating-blade microtome (Leica VT1000s) in artificial cerebrospinal fluid (ACSF: 0.1386 mol L^{-1} NaCl, 3.5×10^{-3} mol L^{-1} KCl, 2.1×10^{-2} mol L^{-1} $NaHCO_3$, 6×10^{-4} mol L^{-1} NaH_2PO_4, 9.9×10^{-3} mol L^{-1} D-glucose, 1×10^{-3} mol L^{-1} $CaCl_2$, and 3×10^{-3} mol L^{-1} $MgCl_2$). Slices were incubated with 4×10^{-5} mol L^{-1} CBT in ACSF bubbled with 95% O_2 and 5% CO_2 for 60 min at 37 °C. Slices were then washed three times with ACSF and transferred to glass-bottomed dishes (NEST) and observed using a two-photon confocal microscope.

2.8. Fluorescence imaging

Two-photon fluorescence imaging was obtained with a LSM 710 NLO (Zeiss) multiphoton laser scanning microscope. The excitation wavelength was 800 nm. Two optical windows (at channel I: 430–480 nm and channel II: 525–575 nm) were observed. Confocal fluorescence imaging was obtained with a LSM 780 (Zeiss) confocal laser scanning microscope. The excitation wavelength was 405 nm. Two optical windows (at channel I: 430–480 nm and channel II: 525–575 nm) were observed.

3. Results and discussions

3.1. Synthesis of CBT

The chemical structure of CBT has been shown in Scheme 1. The pK_a for the conjugated acid of pyridine is about 5.0, so a weakly base pyridine was introduced as the recognition moiety for proton. The synthesis of CBT was with facile and economic methods. Reaction of carbazole and 2-bromoethyl ethyl ether afforded compound 1. Compound 2 was obtained through a Vilsmeier reaction. Then a solution of compound 2 and NBS in chloroform/HOAc was stirred for 15 h to afford compound 3. Under nitrogen compound 4 was obtained through a heck reaction using the reagents compound 3 and 4-vinylpyridine. After stirring Compound 4 and 2-aminobenzenethiol in DMF for overnight, the crude product was obtained and purified by column chromatography. After recrystalization from methanol, CBT was obtained. Through the protonation of pyridine N atom under acidic conditions, the new species (CBT-H^+) can form (Scheme 2).

3.2. Photophysical properties of CBT

Photophysical properties of CBT were investigated in various solvents such as cyclohexane, toluene, ethyl acetate, THF, acetone,

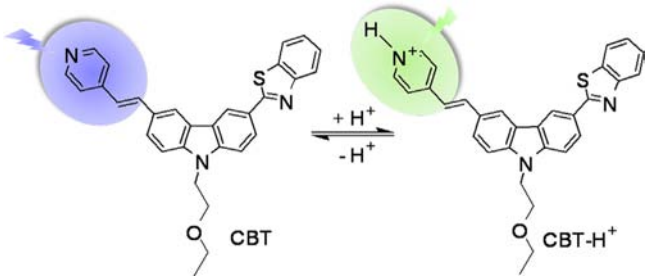

Scheme 2. Structure of CBT and CBT-H^+.

Table 1
Photophysical properties of CBT in various solvents.

Solvent	λ_1(nm)	λ_2(nm)	$\Delta\nu$(nm)	Φ(%)
Cyclohexane	354	384	30	18.33
Toluene	360	399	39	14.27
Ethyl Acetate	359	409	50	12.37
THF	360	420	59	9.47
Acetone	360	426	66	9.48
Acetonitrile	360	438	78	8.67
Buffer (pH 7.4)	370	460	90	4.47
Buffer (pH 4.5)	390	548	158	1.70

λ_1, λ_2 are linear absorption and one-photon fluorescence maximum peaks; $\Delta\nu$ is Stokes shift; Φ is one-photon fluorescence quantum yield; standard is quinine sulfate in 0.5 mol L^{-1} H_2SO_4; concentration of samples: 1×10^{-5} mol L^{-1}.

acetonitrile and buffers (Table 1 and Fig. 1). With organic solvent polarity increased, its absorption maxima showed only a very slight red-shift (354 nm–360 nm), indicating its weak solvent effect. Comparatively, its fluorescence spectra showed a significant bathochromic shift (384 nm–438 nm), indicating that the emission spectra are strongly dependent on the dipole moment of the solvents [25] and that the energy gap between the excitation state and the ground state decreased with increasing solvent polarity. Along with bathochromic shifts, the fluorescence quantum yields decreased (from 0.18 to 0.09), which were attributed to the acceleration of internal conversion [26]. Meanwhile, relative large Stokes shifts (30 nm–78 nm) of fluorescent bands in different solvents are typical of the fluorescence from the relaxed intramolecular charge transfer (ICT) states [27].

On the other hand, the fluorescence quantum yield of CBT in buffer is obviously low in comparison with that in organic solvents. For such dyes, ICT state could occur between the electron donor such as carbazole and thiazole moiety and the electron acceptor such as pyridine and pyridinium cation. Once in buffer containing large numbers of water, the large dipole moment in the excited state than that in the ground state strongly interacts with the polar solvent, which could lead to charge separation resulting in formation of a twist intramolecular charge transfer (TICT) state whose non-radiative process quenches fluorescence. When dyes are protected from water in organic surroundings, its fluorescent will be restored. According to these data and discussions above, we propose that photophysical properties of this probe are due to an ICT mechanism [19].

According to Fig. 2(a), when excited by 405 nm, the peaks of one-photon excited fluorescence (SPEF) red-shifted evidently from 463 nm at pH 7.4 solution to 546 nm at pH 4.5 one, indicating that CBT-H^+ whose structure was shown in Scheme 2 formed. Meanwhile, as shown in Fig. 2(a) inset, the intensity ratios of the two maximum emission peaks ($I_{546\ nm}/I_{463\ nm}$) showed a remarkable enhancement from 0.29 to 6.92 with the gradually reducing of pH value and nonlinear fit of the sigmoidal curve (emission intensity ratios versus pH value) afforded CBT a pK_a value of 4.90. At the same time, as revealed by the absorption measurement (Fig. S1), the linear absorption wavelengths of CBT-H^+ is in the range of 350–440 nm, hence their two-photon absorption can be excited by a Ti: sapphire laser source in the range of 730–880 nm. And the two-photon absorption cross-sections (δ) of CBT and CBT-H^+ are 131 g and 354 g at 800 nm, respectively. In Fig. 2(b), upon the change of pH values in environments, the TPEF peaks of CBT red-shifted clearly from 462 nm at pH 7.4 solution to 571 nm at pH 4.5 one when excited by 800 nm. According to inset in Fig. 2(b), the peak intensity ratios of $I_{571\ nm}/I_{462\ nm}$ showed a remarkable enhancement from 0.85 to 20.10 with the gradually reducing of pH value and the pK_a was 4.95. All these data, such as a 24-fold enhancement of $I_{571\ nm}/I_{462\ nm}$, 109 nm separated between the two emission peaks and the δ values of CBT and CBT-H^+ ranked CBT as one of the best TPEF ratiometric probes.

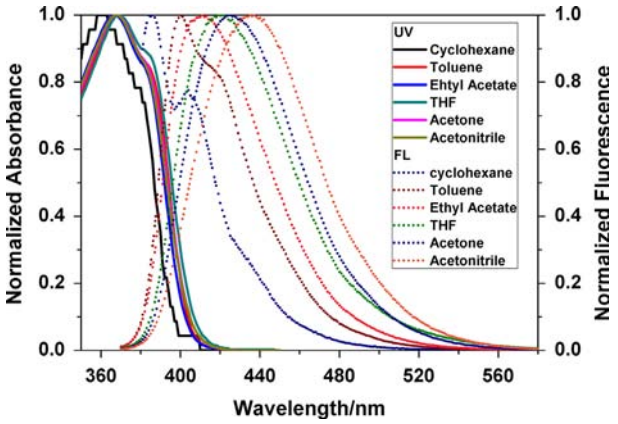

Fig. 1. Normalized absorption and fluorescence spectra of CBT in various solvents. The excitation wavelengths of the fluorescence spectra are the corresponding maximum absorption ones.

3.3. Selectivity and photostability of CBT

On account that the pyridine in CBT may bind various metal cations expressed in cytoplasm and intracellular environment is very complex, its selectivity to H^+ has been investigated. Fortunately, as shown in Fig. 3, the CBT shows its selectivity response to H^+ over metal cations (Al^{3+}, 2×10^{-4} mol L^{-1}; Ca^{2+}, 1×10^{-2} mol L^{-1}; Cd^{2+}, 5×10^{-4} mol L^{-1}; Co^{2+}, 2×10^{-4} mol L^{-1}; Cr^{2+}, 2×10^{-4} mol L^{-1}; Cu^{2+}, 2×10^{-4} mol L^{-1}; Fe^{2+}, 2×10^{-2} mol L^{-1}; Fe^{3+}, 2×10^{-3} mol L^{-1}; Mg^{2+}, 2×10^{-3} mol L^{-1}; Mn^{2+}, 2×10^{-4} mol L^{-1}; Ni^{2+}, 5×10^{-4} mol L^{-1}; Pb^{2+}, 2×10^{-4} mol L^{-1}; Sr^{2+}, 2×10^{-4} mol L^{-1}; Zn^{2+}, 2×10^{-4} mol L^{-1}) and anions (Br^-, 2×10^{-3} mol L^{-1}; NO_3^-, 2×10^{-3} mol L^{-1}; $S_2O_3^{2-}$, 2×10^{-3} mol L^{-1}) in both SPEF and TPEF experiments. At the same time, the competition experiments showed that the addition of bioanalytes above did not result in detectable variation of SPEF and TPEF responses (Fig. 3b and d). The ratio of SPEF ($I_{546\ nm}/I_{463\ nm}$) and TPEF ($I_{571\ nm}/I_{462\ nm}$) of CBT exhibited photostability during 60 min when excited by 405 nm and 800 nm (Fig. S2).

3.4. Two-photon ratiometric fluorescent imaging in HeLa cells

To investigate the utility of CBT as a TPRF probe, its TPEF images in TPM were obtained in HeLa cells incubated with 2×10^{-6} mol L^{-1} CBT for 30 min using 800 nm excitation wavelength and two fluorescent detection channels (I: 430–480 nm and II: 525–575 nm). As shown in Fig. 4(a), (b) and (d), and all HeLa cells incubated with CBT exhibited bright intracellular fluorescence, and no fluorescence is observed in extracellular regions, indicating that CBT is a membrane-permeable probe. At the same time, the differential interference contrast (DIC) images confirmed that the cells were viable throughout the imaging experiments [21].

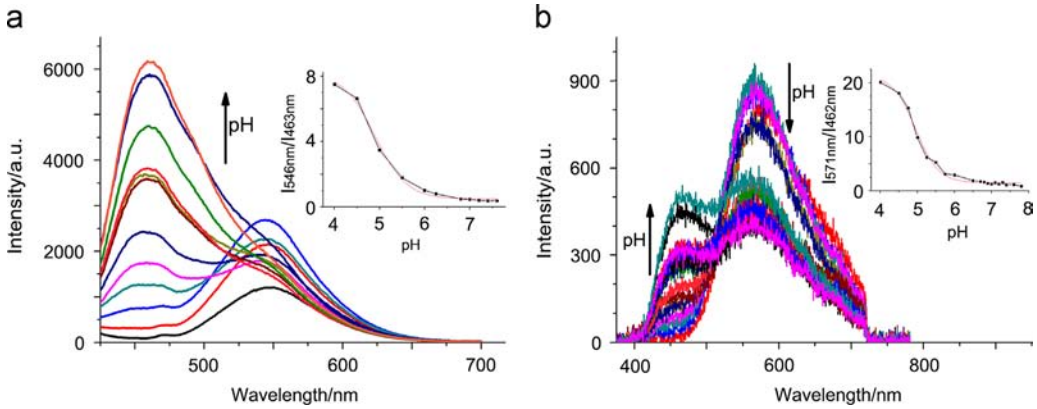

Fig. 2. pH titration of CBT (1×10^{-5} mol L^{-1}) in Britton–Robinson buffer, (*a*): SPEF, λ_{ex}=405 nm, inset: the calibration curve of $I_{546\ nm}/I_{463\ nm}$; (*b*): TPEF, λ_{ex}=800 nm, inset: the calibration curve of $I_{571\ nm}/I_{462\ nm}$.

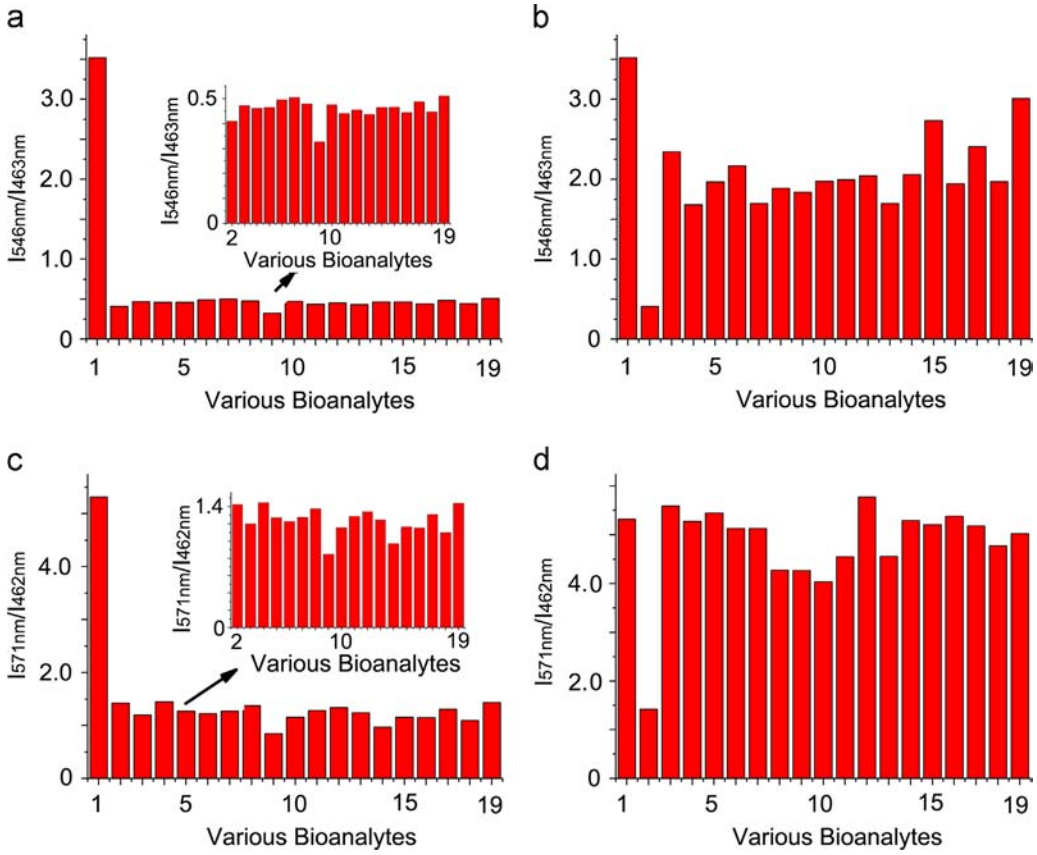

Fig. 3. One-/two-photon fluorescence responses of CBT and CBT-H^+ (1×10^{-5} mol L^{-1}) to various bioanalytes in Britton–Robinson buffer, λ_{ex}=405 nm (a and b), 800 nm (c and d); (a) and (c) 3–19: pH 7.0, (b) and (d) 3–19: pH 5.0. From left to right: 1: CBT-H^+, pH 5.0; 2: CBT, pH 7.0; 3–19: $+Al^{3+}$, $+Ca^{2+}$, $+Cd^{2+}$, $+Co^{2+}$, $+Cr^{2+}$, $+Cu^{2+}$, $+Fe^{2+}$, $+Fe^{3+}$, $+Mg^{2+}$, $+Mn^{2+}$, $+Ni^{2+}$, $+Pb^{2+}$, $+Sr^{2+}$, $+Zn^{2+}$, $+Br^-$, $+NO_3^-$, $+S_2O_3^{2-}$.

Furthermore, the TPEF ratiometric photos of Fig. 4(a) and (b) were presented in Fig. 4(e), and the pH values in ratiometric scale in the right side of Fig. 4(e) may be written according to the inset in Fig. 2 (b) which is basically consistent with inset in Fig. 2(a). Consequently, the spatial coordinates of intracellular pH can be obtained by contrasting intracellular pseudocolor in Fig. 4(e) as well as its partial enlargement with the pseudo-color in the rariometric scale.

3.5. Spatial coordinates determination of intracellular pH

In order to detect the rationality of ratiometric scale in which different colors represent the different pH values, the in situ intracellular calibration experiments were performed in SiHa cells with H^+/K^+ ionophore nigericin [4], which is a standard approach for homogenizing the pH of cytoplasm. In Fig. 5, fluorescent, DIC, merge and ratiometric photos came from normal cells (a)–(e), cells processed with nigericin and 4.5 pH buffers (f)–(j) and cells processed with nigericin and 6.0 pH buffers (k)–(o), respectively. The pH values in ratiometric scale have been written on the basic of the inset in Fig. 2(a). According to the ratiometric scale, pH values of intracellular offwhite domains in Fig. 5(e) should be ~4.5 and pH of azury those should be ~6.0. Delightfully, the experiment results in Fig. 5(j) and (o) confirmed this conclusion: in Fig. 5(j), a majority of intracellular regions presents offwhite and that in Fig. 5(o) is azury.

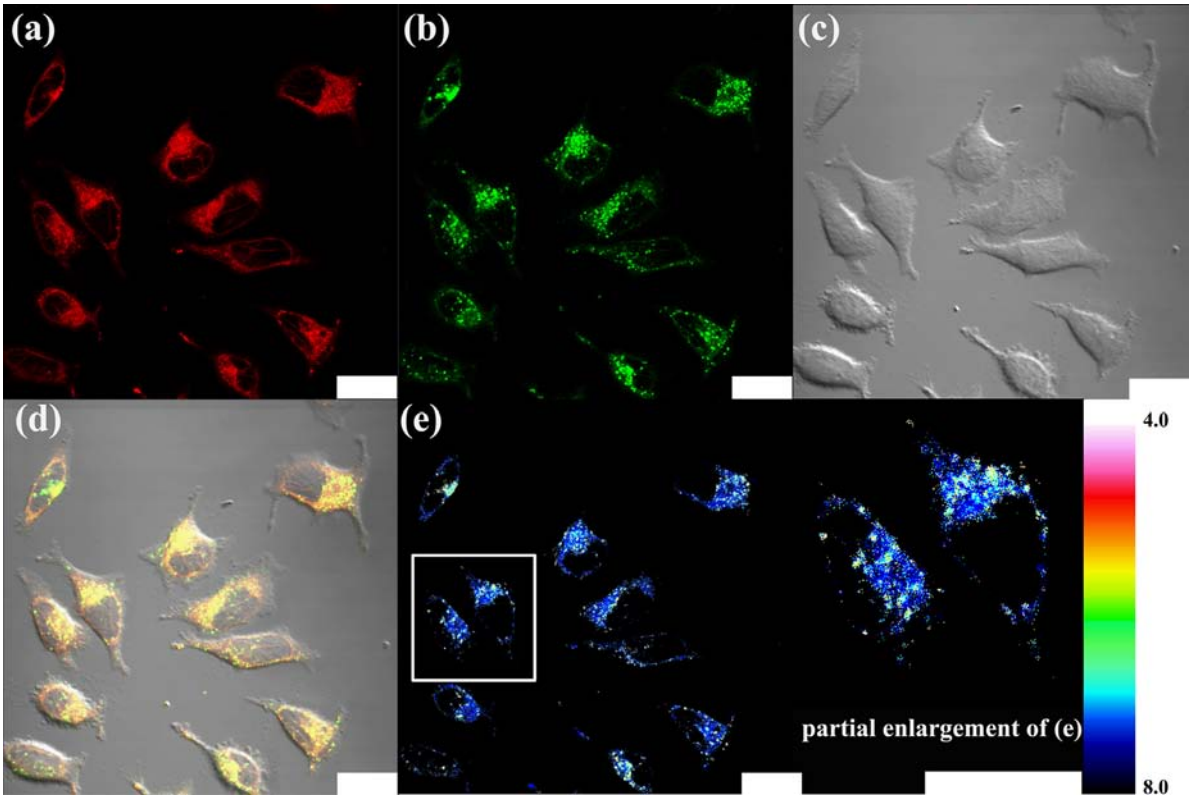

Fig. 4. TPEF images of HeLa cells incubated with 2×10^{-6} mol L^{-1} CBT for 30 min. (a): Channel *I* (430–480 nm); (b): Channel II (525–575 nm); (c): DIC; (d): Overlay of (*a*)-(*c*); (*e*) Ratiomitric images of (*b*) and (*a*); λ_{ex}=800 nm; Bar=20 μm.

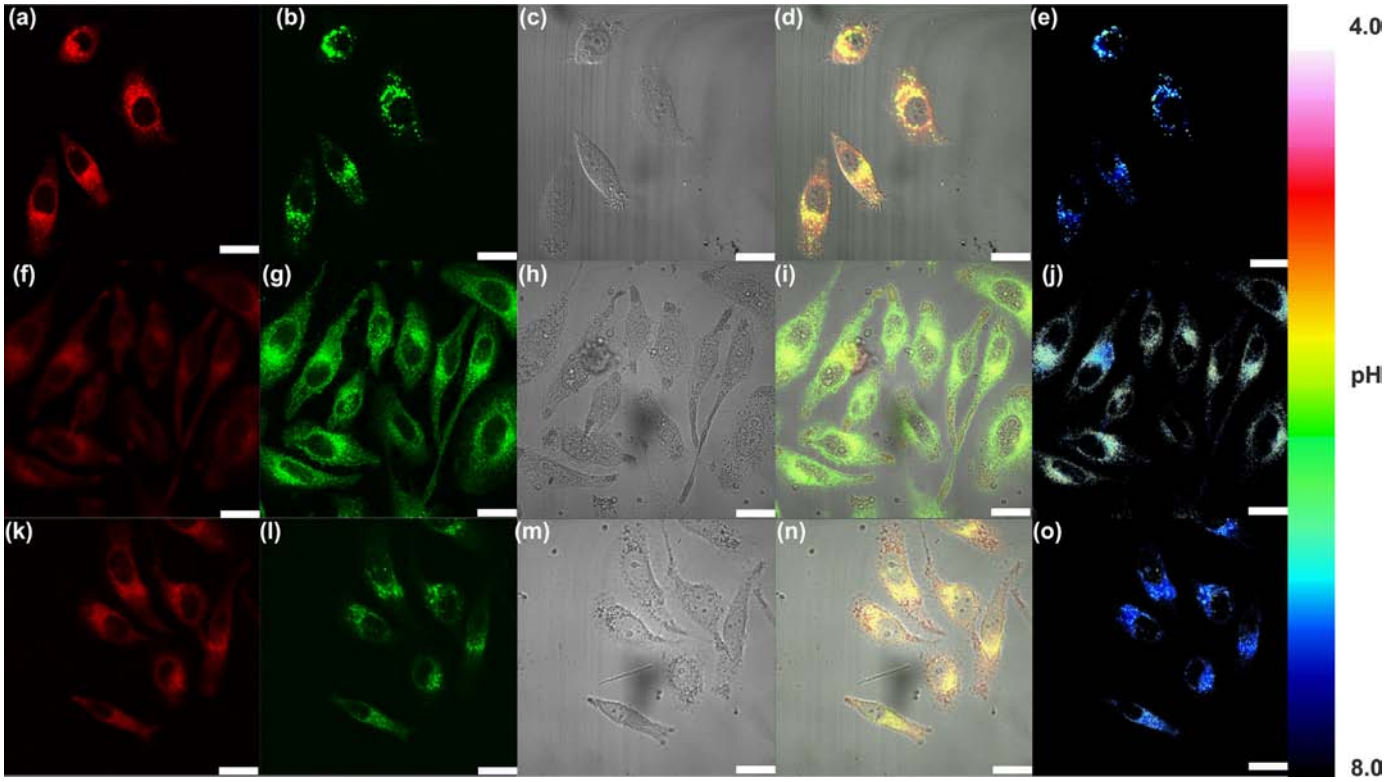

Fig. 5. SPEF images of SiHa cells incubated with 2×10^{-6} mol L^{-1} CBT for 30 min. (a), (f), and (k): Channel *I* (430–480 nm); (b), (g), and (l): Channel II (525–575 nm); (c), (h) and (m): DIC; (d), (i) and (*n*): Overlay of (a)–(c), (f)–(h) and (k)–(m); (e), (j) and (o): Ratiomitric images of (b) and (a), (g) and (f), (l) and (k) respectively; (a)–(c): Images of normal SiHa; (f)–(h) Images of SiHa, pH 4.5; (k)–(m) Images of SiHa, pH 6.0; λ_{ex}=405 nm, Bar=20 μm.

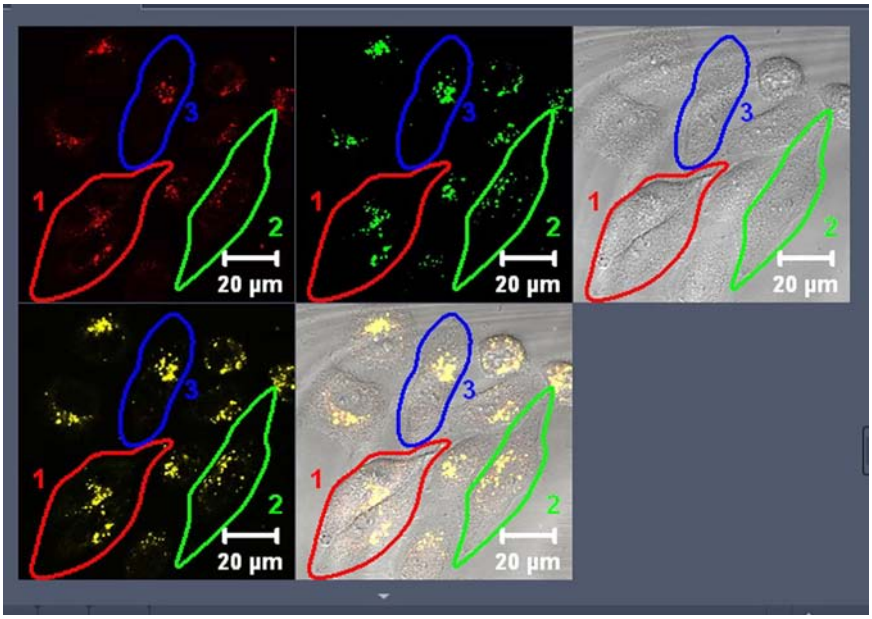

Video S1. Supplementary material related to this paper can be found online at http://dx.doi.org/10.1016/j.talanta.2014.05.039.

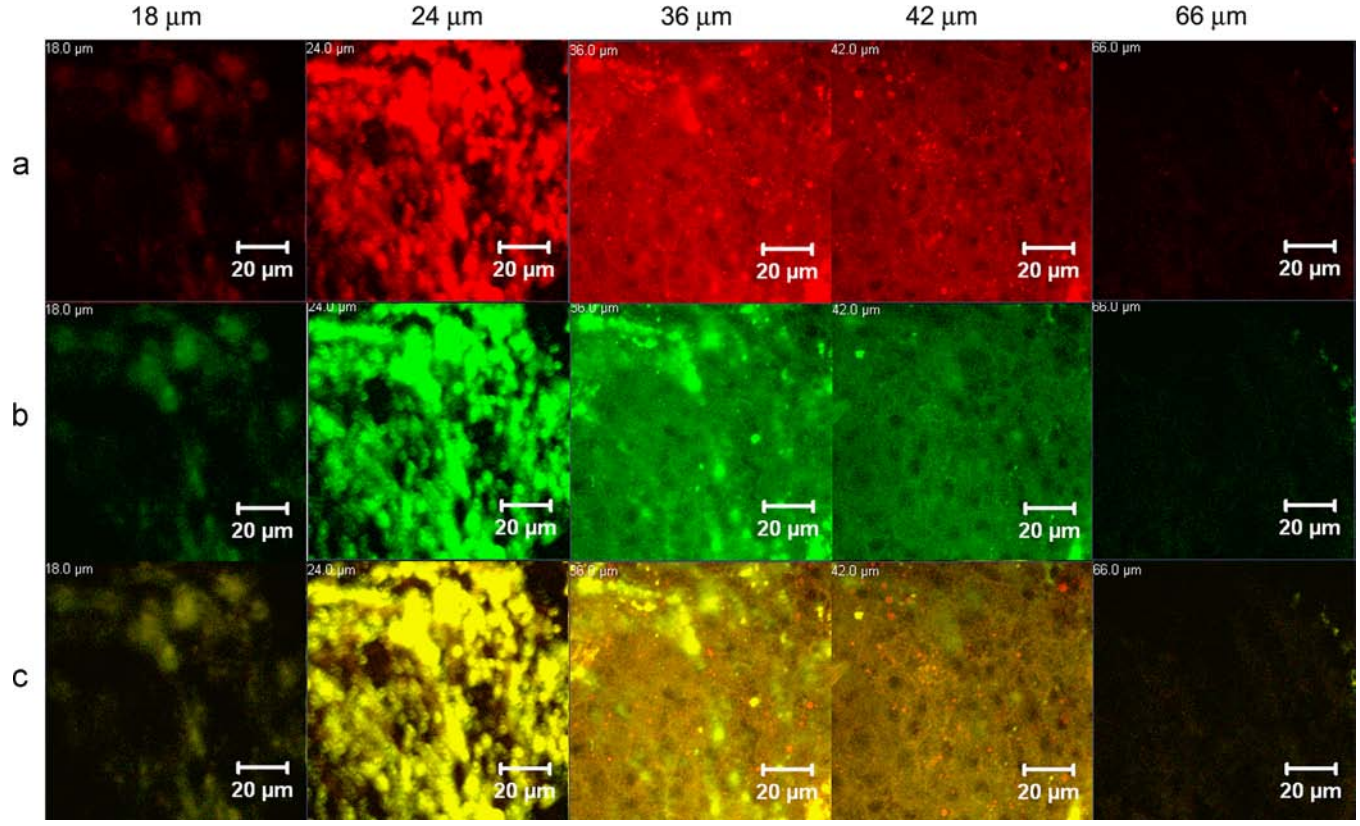

Fig. 6. TPEF images of SD rats (14-day-old, SPF) liver biopsy slices stained with 4×10^{-5} mol L^{-1} CBT for 120 min. (a): Channel *I* (430–480 nm); (b): Channel II (525–575 nm); (c): Overlay of (a) and (b); λ_{ex}=800 nm; Bar=20 μm.

3.6. The permeability to living cells of CBT and its cytotoxicity

A series of the fluorescent images in different incubation time can record the internalization process of CBT to living SiHa cells, and these images constructed Video S1. As shown in Video S1, when excited by 405 nm laser, the intracellular fluorescent intensities from three detection channels (I: 430–480 nm, II: 525–575 nm and III: 430–575 nm) obviously enhanced with time, indicating the concentration of CBT within cells can continually increase. The fluorescent images in 13.6 s and 15 min were presented in Fig. S3 and Fig. S4. In Fig. S3, no intracellular fluorescence was observed, comparatively, one in Fig. S4 was very bright. In order to better explain the permeability of CBT, we randomly selected three regions containing cells in Video S1, and the regions were indicated by numerals (1, 2 and 3) and erose circles (red, green and blue), respectively. The relationship between the fluorescent intensity

from every region of CBT an incubation time was plotted in Fig. S5. According to Fig. S5, one can deduce that the original time in which CBT enters cells should be at 150 s and intracellular CBT can attain saturation at 10 min. These experiment results displayed that CBT possesses better permeability. At the same time, the cytotoxicity of CBT was evaluated in HeLa cells by MTT assay. The cell viability assay data of cells treated with 2×10^{-6} mol L^{-1} and 5×10^{-6} mol L^{-1} CBT at 30 min were showed at Fig. S6, indicating the ratios of survival cells are 88.7% and 86.1% .

3.7. Two-photon fluorescent imaging in rat liver biopsy slices

TPM is superior to traditional confocal microscopy when imaging thick, opaque, living specimen [11]. It is necessary to investigate the utility of CBT in living tissue. Fluorescent imaging of rat liver biopsy slices staining with CBT was surveyed by TPM. Signals of two fluorescent detection channels (I: 430–480 nm and II: 525–575 nm) were collected and the excitation wavelength was 800 nm. At last, the imaging depth of CBT in biopsy slices was investigated in TPM (Fig. 6), and the results showed that its maximum imaging depth can arrive 66 μm in living animal tissues.

4. Conclusions

In this study, we have developed a TPRF pH probe with the GM value of 354 at pH 4.5 and good membrane permeability thus CBT can be introduced into a living cell by simple incubation process. Moreover, the TPEF of CBT can show distinct emission peak shift as large as 109 nm upon the change of pH values in experiment in vitro. And its working pH value range between 4.0 and 8.0 just corresponds to that of intracellular pH. In general, a cell can be divided into two parts based on pH values: neutral cytosol (pH: 6.8–7.4) and acidic compartments (pH: 4.5–6.0) [22]. Fortunately, as a TPRF probe, its excitation wavelength is just at 800 nm, one optimal output of Ti: sapphire femtosecond laser as the routine equipment of recent TPM, so that TPEF ratiometric images of pH could be obtained conveniently and rapidly. Finally, CBT can be applied in TPM and confocal microscopy for imaging in living cells and tissues. Very importantly, both the ratiometric fluorescent imaging and in situ intracellular calibration experiments confirmed that CBT enables spatial coordinates determination of intracellular pH values of living cells. And imaging depth in living biopsy slices is 66 μm in TPM.

Acknowledgment

Our Laser confocal scanning imaging of living cells was performed at The Microscopy Characterization Facility, Shandong University. For financial support, we thank the National Natural Science Foundation of China (51273107 and 51303097), Natural Science Foundation of Shandong Province, China (ZR2012EMZ001), Shandong University 2011JC006, Open Project of State Key Laboratory for Supramolecular Structure and Materials (SKLSSM201419).

Appendix A. Supporting information

Supplementary data associated with this paper can be found in the online version at http://dx.doi.org/10.1016/j.talanta.2014.05.039.

References

[1] J. Han, K. Burgess, Chem. Rev. 110 (2010) 2709–2728.
[2] J. Clayton, C.I. Jack, C. Ryall, J. Tran, E. Hilal, M. Gosney, Age Ageing 35 (2006) 47–53.
[3] H. Izumi, T. Torigoe, H. Ishiguchi, H. Uramoto, Y. Yoshida, M. Tanabe, T. Ise, T. Murakami, T. Yoshida, M. Nomoto, K. Kohno, Cancer Treat. Rev. 29 (2003) 541–549.
[4] C.C. Overly, K.D. Lee, E. Berthiaume, P.J. Hollenbeck, Proc. Natl. Acad. Sci. USA. 92 (1995) 3156–3160.
[5] K.M. Sun, C.K. McLaughlin, D.R. Lantero, R.A. Manderville, J. Am. Chem. Soc. 129 (2007) 1894–1895.
[6] X. Zhang, Y. Xiao, X. Qian, Angew. Chem. Int. Ed. 47 (2008) 8025–8029.
[7] M.A. Haidekker, T.P. Brady, D. Lichlyter, E.A. Theodorakis, J. Am. Chem. Soc. 128 (2006) 398–399.
[8] R. Badugu, J.R. Lakowicz, C.D. Geddes, Talanta 66 (2005) 569–574.
[9] P. Carol, S. Sreejith, A. Ajayaghosh, Chem. Asian J. 2 (2007) 338–348.
[10] A. Hakonen, S. Hulth, S. Dufour, Talanta 81 (2010) 1393–1401.
[11] S.M. Potter, Curr. Biol. 6 (1996) 1595–1598.
[12] N. Zhao, Y. Zhang, X. Liu, X. Yu, M. Ge, Chin. Sci. Bull. 55 (2010) 3661–3667.
[13] S. Charier, O. Ruel, J.B. Baudin, D. Alcor, J.F. Allemand, A. Meglio, L. Jullien, Angew. Chem. Int. Ed. 43 (2004) 4785–4788.
[14] H.J. Park, C.S. Lim, E.S. Kim, J.H. Han, T.H. Lee, H.J. Chun, B.R. Cho, Angew. Chem. Int. Ed. 51 (2012) 2673–2676.
[15] P.D. Jobsis, C.A. Combs, R.S. Balaban, J. Microsc. 217 (2005) 260–264.
[16] T.V. Esipova, X. Ye, J.E. Collins, S. Sakadžić, E.T. Mandeville, C.B. Murray, S.A. Vinogradov, Proc. Natl. Acad. Sci. U.S.A. 109 (2012) 20826–20831.
[17] S. Yao, K.J. Schafer-Hales, K.D. Belfield, Org. Lett. 9 (2007) 5645–5648.
[18] H.J. Kim, C.H. Heo, H.M. Kim, J. Am. Chem. Soc. 135 (2013) 17969–17977.
[19] Y. Zhang, J. Wang, P. Jia, X. Yu, H. Liu, X. Liu, N. Zhao, B. Huang, Org. Biomol. Chem. 8 (2010) 4582–4588.
[20] G. Song, F. Miao, Y. Sun, X. Yu, J.Z. Sun, W.Y. Wong, Sens. Actuator B: Chem. 173 (2012) 329–337.
[21] Z. Yang, N. Zhao, Y. Sun, F. Miao, Y. Liu, X. Liu, Y. Zhang, W. Ai, G. Song, X. Shen, X. Yu, J. Sun, W.Y. Wong, Chem. Commun. 48 (2012) 3442–3444.
[22] F. Miao, G. Song, Y. Sun, Y. Liu, F. Guo, W. Zhang, M. Tian, X. Yu, Biosens. Bioelectron. 50 (2013) 42–49.
[23] A.N. Fletcher, Photochem. Photobiol. 9 (1969) 439–444.
[24] M.A. Albota, C. Xu, W.W. Webb, Appl. Opt. 37 (1998) 7352–7356.
[25] A.P. de Silva, H.Q.N. Gunaratne, T. Gunnlaugsson, A.J.M. Huxley, C.P. McCoy, J.T. Rademacher, T.E. Rice, Chem. Rev. 97 (1997) 1515–1566.
[26] A. Loudet, K. Burgess, Chem. Rev. 107 (2007) 4891–4932.
[27] S.A. Jenekhe, L. Lu, M.M. Alam, Macromolecules 34 (2001) 7315–7324.